Prevalence of updip rupture propagation in interplate earthquakes along the Japan Trench

Keisuke Yoshida[1], Naoki Uchida[1], Hisahiko Kubo[2], Ryota Takagi[1], and Shiqing Xu[3]

[1]Tohoku University
[2]National Research Institute for Earth Science and Disaster Resilience, Tsukuba, Japan
[3]Southern University of Science and Technology

November 22, 2022

Abstract

The development of seafloor seismic observations facilitates reliable estimation of the rupture directivities of offshore earthquakes. We used seismic waveforms obtained by a new seafloor seismic network (S-net) and onland stations to systematically examine the rupture directivities of interplate earthquakes along the Japan trench. We estimated the rupture directions of 206 (M w 3.5-5) events, most of which occurred near the base of the seismogenic zone. We found that most earthquake ruptures (>~80 %) were directional, primarily propagating in the updip direction. This tendency cannot be explained by the effect of the bimaterial interface. The prevalence of updip rupture in the data suggests that deep, steady creep and upward fluid migration along the plate interface affected earthquake ruptures in the subduction zone. The updip ruptures redistributed the accumulated shear stress from the base of the seismogenic zone to the shallow large seismic patches. Furthermore, the updip ruptures may open up ways for deeper fluids to migrate further upward along the plate interface. Both the stress redistribution and the upward fluid migration facilitate the occurrence of shallow megathrust earthquakes.

Hosted file

`essoar.10507292.1.docx` available at https://authorea.com/users/533568/articles/599552-prevalence-of-updip-rupture-propagation-in-interplate-earthquakes-along-the-japan-trench

Prevalence of updip rupture propagation in interplate earthquakes along the Japan Trench

Keisuke Yoshida[1], Naoki Uchida[1], Hisahiko Kubo[2], Ryota Takagi[1], Shiqing Xu[3]

[1] Research Center for Prediction of Earthquakes and Volcanic Eruptions, Graduate School of Science, Tohoku University, Sendai, Japan

[2] National Research Institute for Earth Science and Disaster Resilience, Tsukuba, Japan

[3] Department of Earth and Space Sciences, Southern University of Science and Technology, Shenzhen, China

Corresponding author: Keisuke Yoshida, Research Center for Prediction of Earthquakes and Volcanic Eruptions, Tohoku University, 6-6 Aza-Aoba, Aramaki, Aoba-Ku, Sendai, 980-8578, Japan (keisuke.yoshida.d7@tohoku.ac.jp)

Submitted on Feb. 11, 2021

Abstract (175 words)

The development of seafloor seismic observations facilitates reliable estimation of the rupture directivities of offshore earthquakes. We used seismic waveforms obtained by a new seafloor seismic network (S-net) and onland stations to systematically examine the rupture directivities of interplate earthquakes along the Japan trench. We estimated the rupture directions of 206 (M_w 3.5–5) events, most of which occurred near the base of the seismogenic zone. We found that most earthquake ruptures (>80 %) were directional, primarily propagating in the updip direction. This tendency cannot be explained by the effect of the bimaterial interface. The prevalence of updip rupture in the data suggests that deep, steady creep and upward fluid migration along the plate interface affected earthquake ruptures in the subduction zone. The updip ruptures redistributed the accumulated shear stress from the base of the seismogenic zone to the shallow large seismic patches. Furthermore, the updip ruptures may open up ways for deeper fluids to migrate further upward along the plate interface. Both the stress redistribution and the upward fluid migration facilitate the occurrence of shallow megathrust earthquakes.

Keywords

Rupture directivity, Interplate earthquake, Japan trench, Deep creep, Fluid migration, Subduction zone

Submitted on Feb. 11, 2021

1. Introduction

A physical understanding of earthquakes involves not only the static characteristics of the rupture, but also the dynamics. Earthquake ruptures are often approximated by symmetrical expansions of circular fault patches (e.g., Sato and Hirasawa, 1973). However, according to systematic investigations, many earthquake ruptures propagate asymmetrically (McGuire et al., 2002; Chounet et al., 2018; Yoshida, 2019). Rupture directivity is a fundamental characteristic of earthquake growth and is essential for improving our current physical understanding of earthquakes. Besides, rupture directivity provides information regarding the stress redistribution process that occurs along the fault.

The effect of material contrast across a fault interface (bimaterial effect) has received attention for its role in understanding earthquake rupture direction (Weertman, 1980; Shi and Ben-Zion, 2006). When an in-plane subshear rupture propagates in the slip direction of the compliant side, a dynamic reduction in normal stress occurs, leading to a lower frictional resistance and hence a higher rupture velocity in this direction. The bimaterial effect leads to a hypothesis that a preferable rupture direction may exist, controlled by the bimaterial effect which is independent of the earthquake size. Some reports have concluded that the observed dominant rupture direction of small earthquakes on the San Andreas fault is consistent with the prediction derived from the bimaterial effect (e.g., Lengline and Got, 2010; Kane et al., 2013). However, others argue that effects other than the bimaterial effect, such as spatial variations in background stress, play more crucial roles in earthquake rupture directivity (Harris and Day, 2005; Kane et al., 2013). It is important to assess the above hypothesis by incorporating reliable data from different tectonic settings as this hypothesis is involved in predicting the rupture directions of future earthquakes. Currently, the rupture characteristics of interplate earthquakes have been

Submitted on Feb. 11, 2021

examined in detail, mostly for a small number of large earthquakes in subduction zones (Yamanaka and Kikuchi, 2004; Ye et al., 2016). However, the rupture characteristics of a large amount of small- to moderate-sized earthquakes have not been thoroughly studied, despite their potential to improve the significance level of the direction estimates by increasing the sample size. The reliability of the rupture-direction measurement of small earthquakes, however, highly depends on the azimuthal coverage of observations. Poor azimuthal coverage makes the reliable estimation difficult. Interplate earthquakes in subduction zones mostly occur beneath the ocean, where seismic stations are usually scarce, causing a paucity of data.

The present study systematically estimates the rupture directivity of interplate earthquakes (Mw 3.5–5) along the Japan trench to investigate earthquake rupture dynamics. Many large earthquakes have occurred along the Japan trench and caused disasters in Japan, including the 2011 M 9 Tohoku-Oki earthquake. Recently, Seafloor observation network for earthquakes and tsunamis along the Japan Trench (S-net), was installed along the Japan trench by the National Research Institute for Earth Science and Disaster Resilience (NIED) (Fig. 1a; Aoi et al., 2020). Seismic waveform data from September 2016 onwards are available online (https://www.seafloor.bosai.go.jp/). Fig. 1 (a) shows the distribution of S-net stations, surrounding the epicenters of the recent interplate earthquakes. Waveform records from the S-net and onland stations provide unique observations with good azimuthal coverage for interplate earthquakes occurring beneath the ocean. It is thereby possible to systematically examine the rupture directivity of small earthquakes along the Japan trench.

Submitted on Feb. 11, 2021

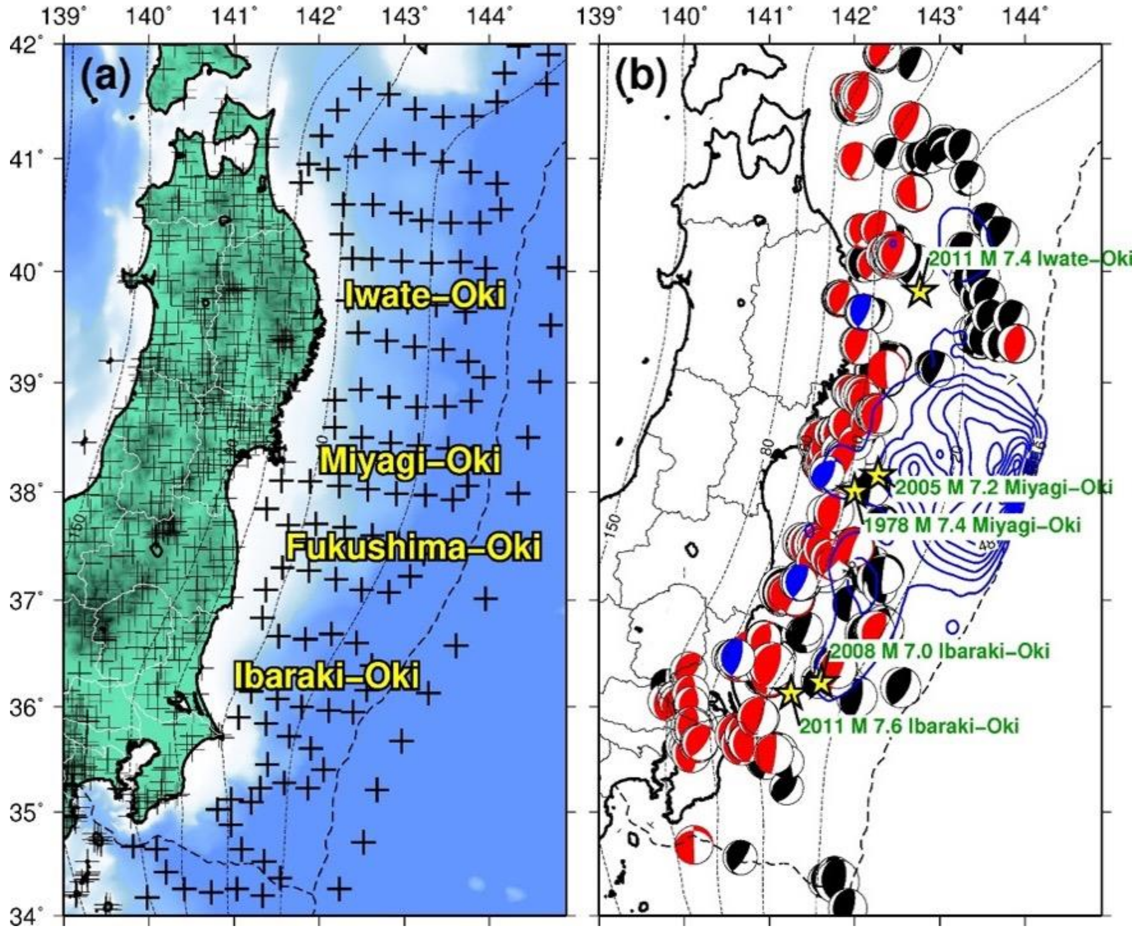

Fig. 1. The distribution of earthquakes and seismic stations in the study area. (a) Distribution of onland and S-net seismic stations. The thick and thin cross indicates S-net stations and onland stations, respectively. (b) Distribution of earthquake focal mechanisms is indicated by beach balls. Red beach balls indicate earthquakes for which rupture parameters were estimated, while black beach balls indicate earthquakes for which rupture parameters were not estimated. Blue beach balls indicate earthquakes for which the results are shown in Fig. 2. The contour lines in blue denote the coseismic slip distribution of the 2011 Tohoku-Oki earthquake determined by Iinuma et al. (2012). Yellow stars represent the five M>7 interplate earthquakes (1978 M 7.4 Miyagi-Oki, 2005 M 7.2 Miyagi-Oki, 2008 M 7.0 Ibaraki-Oki, 2011 M 7.4 Iwate-Oki, and 2011 M 7.6 Ibaraki-Oki

earthquakes) that occurred near the earthquakes analyzed in this study. Dotted contours indicate the depth to the upper plate interface of the subducting Pacific plate, from Nakajima et al. (2009) and Kita et al. (2010).

2. Data and Methods

This study incorporates waveforms obtained from the seismic network composed of stations from the Japan Meteorological Agency (JMA), national universities, Hi-net (NIED, 2019a), F-net (NIED, 2019b), V-net (NIED, 2019c), and S-net (NIED, 2019d), as shown in Fig. 1(a), after removing the instrument responses. Initially, interplate earthquakes were selected (section 2.1) and the apparent moment rate functions (AMRFs) were estimated, based on the empirical Green’s function (EGF) (section 2.2). Next, the rupture direction was estimated by fitting the simple rupture model described by Haskell (1964) to the duration of the AMRFs (section 2.3).

2.1. Selection of interplate earthquakes

The F-net moment tensor catalog (https://www.fnet.bosai.go.jp/event/dreger.php?LANG=en) and JMA unified earthquake catalog (https://www.data.jma.go.jp/svd/eqev/data/bulletin/hypo_e.html) were used to select the interplate earthquakes. The F-net moment tensor catalog lists the moment tensors of earthquakes with M_w greater than about 3.5 in and around Japan, while the JMA unified catalog includes location data for earthquakes with smaller magnitudes. The data period extended from August 2016 to December 2019, for which the S-net station seismograms were also available.

In total, 420 interplate events (target events) were selected using the F-net moment tensors based on the criteria used by Asano et al. (2011) and Hasegawa et al. (2012). The requirements

Submitted on Feb. 11, 2021

were as follows: a rake angle of > 0°, a focal mechanism 3-D rotation angle (Kagan, 1991) relative to that of a reference interplate earthquake (strike: 195°, dip: 15°, rake: 90°) of < 35°, and a depth separation of < 20 km between the centroid and the plate interface (Nakajima et al., 2009). To estimate the directivity of the target events, 660 earthquakes were selected and their waveform data were used for waveform deconvolution (EGF events). These EGF events satisfied the following two criteria: (1) the hypocentral distance from the target event was < 3.0 km according to the JMA unified catalog, and (2) the magnitude was 1–2 magnitudes smaller than the target earthquake. Each target earthquake may have multiple EGF events. Note that the hypocenter locations of the offshore earthquakes had relatively large estimation errors, and thus, earthquakes located far from the target earthquake may sometimes be selected as EGF events. However, these were removed during the waveform deconvolution procedure, as described in section 2.2.

2.2. Determination of the apparent moment rate function and source duration

For waveform deconvolution, we followed the procedure of Yoshida (2019), which adopted the method of Ligorría and Ammon (1999). The transverse components of direct S-waves were used. The orientations of the S-net seismometers determined by Takagi et al. (2019) were used. We first applied a low pass filter to the waveforms of the target and the EGF events. The cut-off frequency (f_l) should be higher than the source corner frequency of the target earthquake. Based on the source model of Sato & Hirasawa (1973), the source corner frequency of S-wave is related to the stress drop $\Delta\sigma$ as follows:

$$f_{\mathrm{cS}}(\Delta\sigma) = kV_s\left(\frac{16}{7}\frac{\Delta\sigma}{M_0}\right)^{\frac{1}{3}} \quad (1)$$

Where, V_s is the S-wave velocity and M_0 is the seismic moment. We assumed $k = 1.9$

corresponding to the situation where the rupture speed is 0.9 times V_s. The typical value of stress drop, $\Delta\sigma$ of interplate earthquakes is 3 MPa (Kanamori & Anderson, 1975). We used $f_\mathrm{l} = f_{\mathrm{cS}}(\Delta\sigma = 50\ \mathrm{MPa})$. Thus, f_l is sufficiently higher than the typical source corner frequency of interplate earthquakes $f_{\mathrm{cS}}(\Delta\sigma = 3\ \mathrm{MPa})$.

The AMRFs were then derived by deconvoluting the waveforms of the target events using the EGFs with a positive value constraint. Synthetic waveforms for the target events can be obtained by convoluting the derived AMRFs with the EGFs. When a synthetic waveform does not reproduce the observed waveform adequately, it implies that the EGF was inappropriate for the observed waveform. Waveform deconvolution thereby naturally removes such inappropriate EGFs (Abercrombie, 2014). Synthetic waveform which reproduced less than 80% of the observed waveform measured in the variance reduction was discarded. If the number of AMRFs from a single EGF event were less than eight, we discarded the AMRFs from that event. The corner frequency (Andrews, 2013) f_c for each AMRF was computed and the apparent source durations were obtained $T_d = \frac{1}{2f_c}$.

Figs. 2 and S1 denote examples of the azimuthal distributions of the AMRFs and the source durations. AMRFs were obtained from more than 15 different stations for 206 of the initial 420 target earthquakes (Fig. S2), and their rupture directivities were examined in detail. The rupture directions of the remaining 214 earthquakes could not be estimated owing to an insufficient number of stations with available AMRFs. For the 214 events, the minimum distances of the EGF events tended to be larger (> 1.5 km) than those of the other 206 events (0–1.5 km) (Fig. S2). This tendency implies that the scarcity of AMRFs for the 214 events was caused by the absence of an appropriate EGF event, probably because the candidate EGF events were too far to assume the same path effect. This natural selection of analyzed events does not bias the statistical tendency of

Submitted on Feb. 11, 2021

the rupture directions because the presence or absence of nearby (< 1.5 km) small events is not related to the rupture direction.

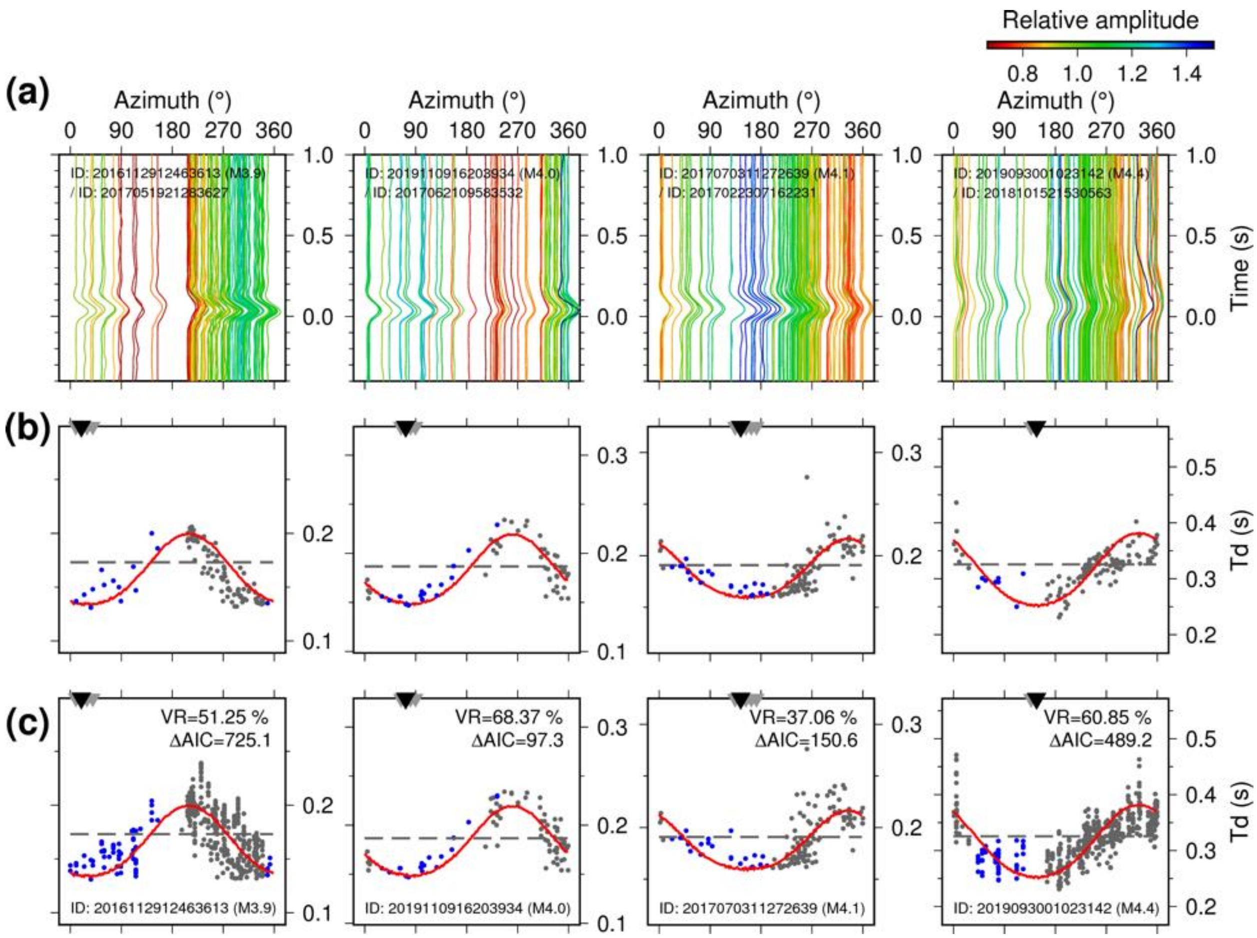

Fig. 2. (a) Examples of the AMRF azimuthal distributions for events shown in Fig. 1(b) from north to south. The different colors indicate the relative maximum amplitude as per the scale provided on the top. (b), (c) Examples of AMRF corner frequencies from a single EGF event and those compiled from multiple EGF events, respectively. Azimuth is measured in degrees, clockwise from the north. Blue dots indicate the results from S-net stations, and gray dots indicate those from onland stations. Black triangles indicate the best-fit azimuth of rupture propagation based on the

unilateral rupture model. Gray triangles indicate the results from bootstrap re-sampling. The red curve and the dashed gray line indicate the computed azimuthal dependences of the corner frequency from the best-fit unilateral model and the non-directional model, respectively. Event IDs (from the JMA catalog) are shown in the lower-left corner of each frame with the moment magnitude (from the F-net catalog).

2.3. Determination of rupture directivity

To estimate the rupture directivity, we followed the procedure described by Yoshida et al. (2019), which uses the 1-D unilateral rupture model (Haskell, 1964) to compute the apparent rupture duration:

$$T_{\mathrm{d0}}{}^{model} = T_0\left(1 - \eta\vec{R}\cdot\vec{U}\right). \tag{2}$$

Where, T_0 is the actual rupture duration, η is the speed of the unilateral rupture divided by V_{S}, and $\vec{R}$ and $\vec{U}$ represent the unit vectors of the rupture propagation and the ray direction at the source, respectively. The shape of a theoretical AMRF is assumed to be a symmetrical triangle with the base of $T_{\mathrm{d0}}{}^{model}$. We applied the same low pass filter to the synthetic triangle and obtained the duration $T_{\mathrm{d}}{}^{model}$ as the same way used for observed AMRFs.

We grid-searched for the combination of $\vec{R}$, T_0, and η that best explained the obtained apparent source durations. $\vec{R}$ was searched on the west-dipping nodal planes of focal mechanisms that corresponded to the plate boundary. The evaluation function is as follows:

$$Var_{\mathrm{uni}} = \frac{\sum_{i=1}^{n}\left(T_{\mathrm{d}}{}^{model}\left(T_0, \eta, \vec{R}, \vec{U_{\mathrm{i}}}\right) - T_{\mathrm{d_i}}\right)^2}{n} \tag{3}$$

where $T_{\mathrm{d_i}}$ and $\vec{U_{\mathrm{i}}}$ are T_{d} and $\vec{U}$, respectively, of the i-th AMRFs, and n is the number of the AMRFs. $\vec{U_{\mathrm{i}}}$ was computed based on the 1-D velocity model of Ueno et al. (2002). We changed the apparent speed ratio η (0–1.0) by dividing the interval by 0.05, and the rupture propagation direction (10–360°) that determined $\vec{R}$ by dividing the interval by 10°. The rupture duration T_0 was searched from 100 points, evenly dividing the interval on a logarithmic scale between 0.1 and ten times the mean value of T_{d_i}. Ruptures may propagate faster than the S-wave velocity in the Mode II direction (Andrews, 1976). However, we considered the likelihood of $\eta > 1$ to be low because Var_{uni} increased beyond $\eta = 1$ for almost all cases in the dataset used in this study.

The residual of Eq. (3) was compared with that of the constant source duration $\overline{T_d}$ case (we referred to the model as the "non-directional model").

$$Var_{\mathrm{mean}} = \frac{\sum_{i=1}^{n}\left(\overline{T_{\mathrm{d}}} - T_{\mathrm{d}_i}\right)^2}{n} \tag{4}$$

$$VR = 100\ \% \times \left(1 - \frac{Var_{\mathrm{uni}}}{Var_{\mathrm{mean}}}\right) \tag{5}$$

If a unilateral rupture more suitably models the duration data, VR will approach 100%. $\overline{T_d}$ was determined during the above grid-search procedure (best-fit value when $\eta = 0$).

We computed the Akaike Information Criterion (AIC) (Akaike, 1974) by assuming that measurement errors in the apparent duration followed a Gaussian distribution, as $AIC = n \ln 2\pi + n \ln Var + 2(m+1)$. Var and m are the mean squared residual and the number of model parameters, respectively. $m = 1$ and $m = 3$ was assumed for the non-directional model and the unilateral rupture model, respectively. We computed the difference $\Delta AIC = AIC_{mean} - AIC_{uni}$, where AIC_{mean} and AIC_{uni} are the AICs of the non-directional model and the unilateral rupture model, respectively.

We estimated the uncertainty range of the directivity parameters for each earthquake by conducting the above procedure on 1,000 simulated datasets based on bootstrap re-sampling of the duration data. We determined the 95% confidence intervals of $\vec{R}$, T_0, and η. Figs. 2(b) and (c) include examples of the best-fit values and 95% confidence intervals of the rupture azimuths determined using this method.

3. Results

We obtained the rupture parameters for 206 earthquakes (Mw 3.5–5), for which the $\Delta AICs$ are shown in Fig. 3 (a) by their frequency distribution. ΔAIC was positive in 186 out of the 206 earthquakes, indicating that 186 earthquakes were better modeled by the unilateral rupture model than by the non-directional model. $\Delta AIC > 2$ in 178 earthquakes; that is, the unilateral rupture model was a better model for these earthquakes based on the 95% confidence interval (Yoshida, 2019). For the 178 events with $\Delta AIC > 2$, VR was larger than 25% for ~75% of the events, and VR was larger than 40% for ~40% of the events (Fig. 3b). The mean ΔAIC decreased with an increasing maximum azimuthal gap of the duration data (Fig. 3c), implying that $\Delta AIC < 0$ does not necessarily reflect a non-directional event, but is due to limited data available for resolving the directivity effect.

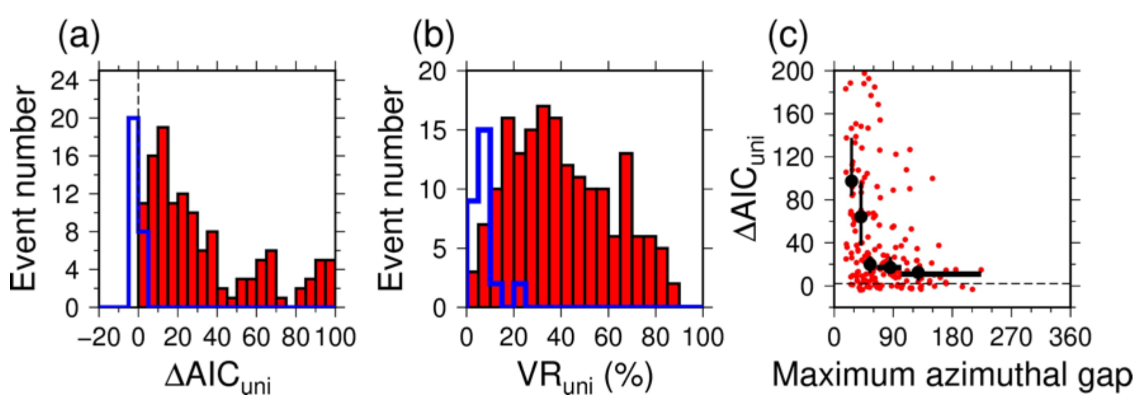

Fig. 3. Results of applying the unilateral rupture model to the dataset used in this study. (a) and (b): Frequency distributions of ΔAIC and VR, respectively. The red bars denote the results with $\Delta AIC > 2$ and blue bars denote those with $\Delta AIC < 2$ (including negative values). (c): Relationship

between ΔAIC and the maximum azimuthal gap of the corner frequency data used to estimate the rupture parameters. Vertical lines indicate 95% confidence intervals of the median value based on bootstrap re-sampling in each bin with the same number of events (n=41). Horizontal lines indicate the ranges of the maximum azimuthal gap in each bin.

Fig. 4 shows the obtained rupture parameters for events with $\Delta AIC > 2$. The estimated value of η is shown in Figs. 4(a) and (b) when the 95 % confidence interval was less than 0.2. η mostly ranged from 0.1 to 0.6 (Fig. 4a). η was variable, and the number of samples for the larger earthquakes were smaller than others, but may have had a tendency to decrease with the moment magnitude (Fig. 4b). Source duration T_0 mostly ranged from 0.1 to 1 s and increased by the power of 1/3 of the seismic moment (Fig. 4c). This relationship is consistent with the self-similarity of earthquakes (Aki, 1967). No clear dependence of the characteristic source duration $T_0/{M_0}^{\frac{1}{3}}$ on the centroid depth was obtained (Fig. 4d).

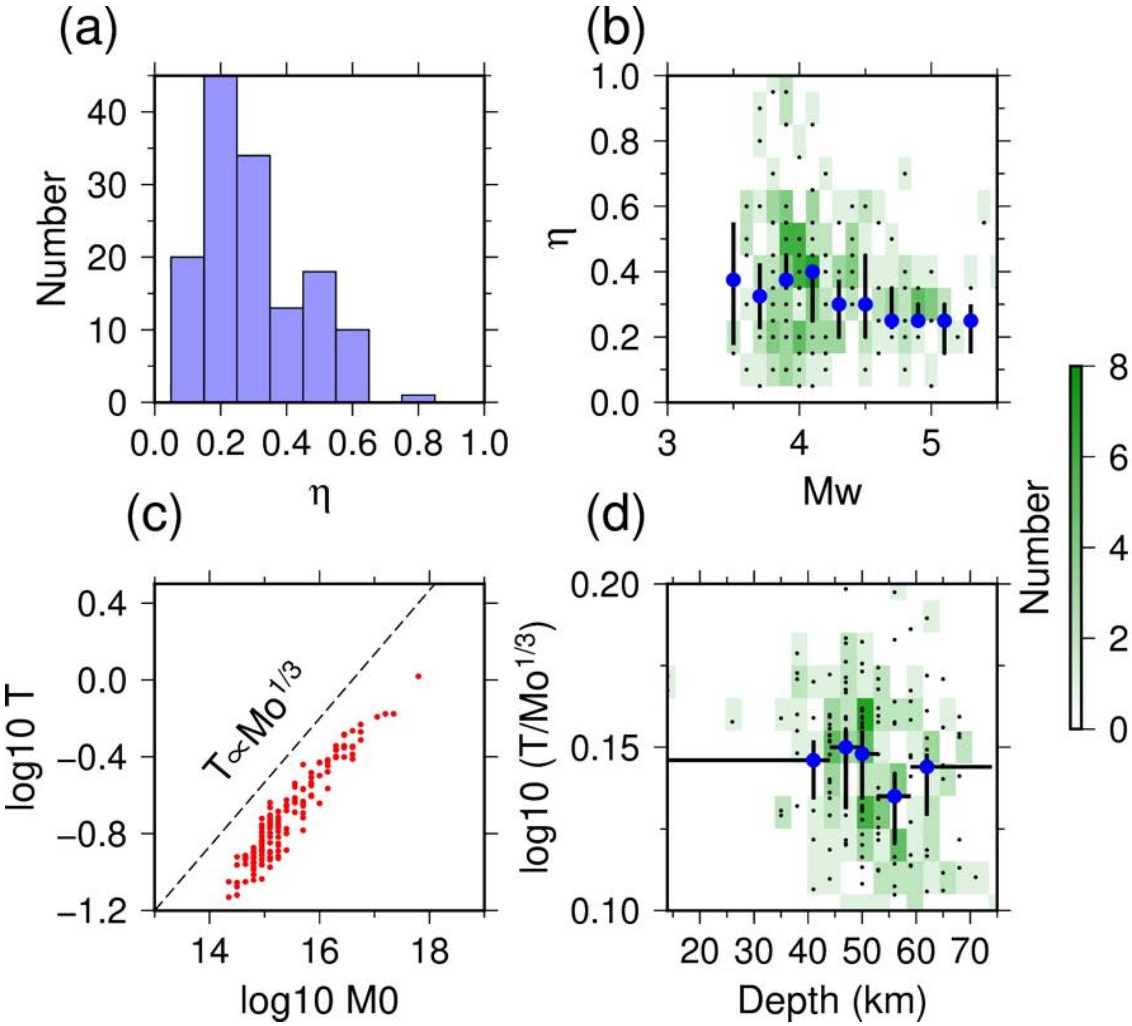

Fig. 4. Derived rupture parameters. Only results with $\Delta AIC > 2$ are shown. (a): Frequency distribution of η. (b): Relationship between η and the moment magnitude. (c): Relationship between seismic moment M_0 and source duration T_0. (d): Relationship between the characteristic source duration $T_0/M_0^{\frac{1}{3}}$ and the centroid depth. Blue circles and vertical lines in (b) and (d) indicate mean values and 90% confidential intervals based on bootstrap re-sampling in each bin with the same number of events, respectively. Horizontal lines indicate the depth ranges in the bins. The color scale indicates the number of samples in (b) and (d).

A clear tendency for the rupture propagation direction was observed. Fig. 5 shows the rupture propagation directions of the 148 earthquakes that satisfied the following two conditions: the 95 % confidence interval of the rupture propagation direction was less than 45° and $\Delta AIC > 2$. The frequency distribution (Fig. 5a) indicates that ruptures of most of the analyzed earthquakes (~80%) were oriented eastward rather than westward. The ruptures of most of the interplate earthquakes along the Japan trench propagated in the updip direction. This tendency appears to be independent of earthquake magnitude (Fig. 5b) and centroid depth (Fig. 5c), and barely changes, even if different criteria were adopted for showing the results. Fig. S3 shows 178 results with a 95% confidence interval for a rupture azimuth of less than 90° regardless of ΔAIC and Fig. S4 shows 114 results with a 95% confidence interval for a rupture azimuth of less than 45° and $\Delta AIC > 20$.

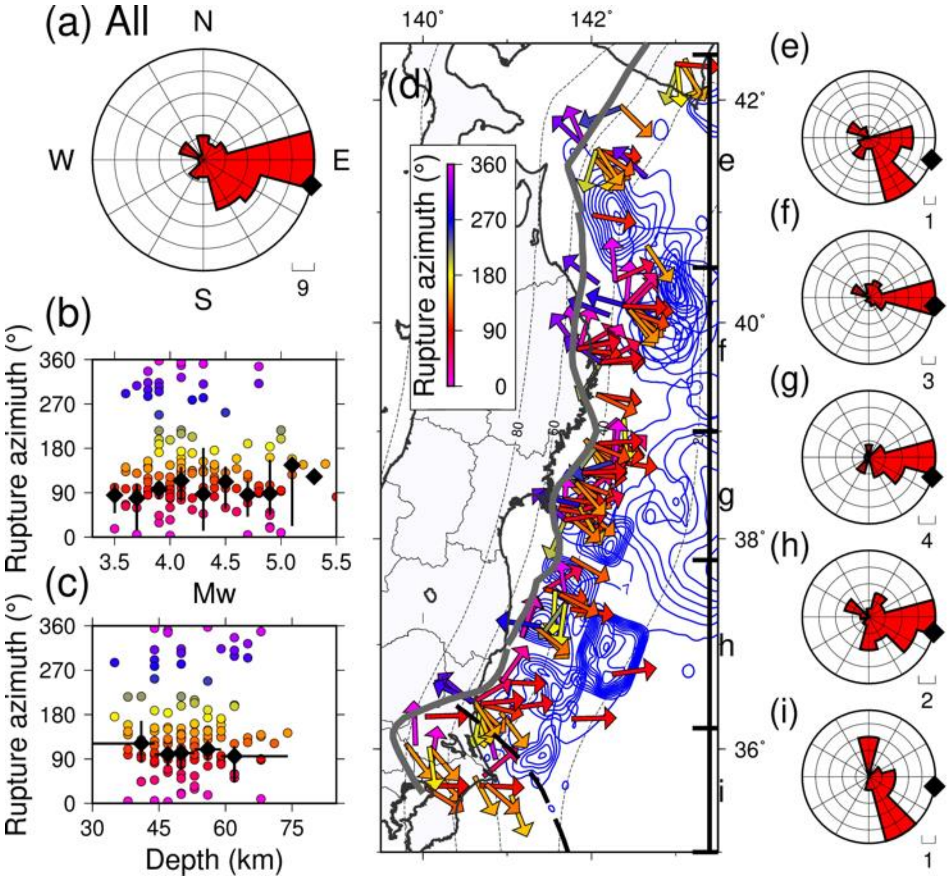

Fig. 5. Estimated rupture propagation directions. Results are indicated for events with a 95% confidence interval of less than 45° and $\Delta AIC > 2$. (a): Frequency distribution of the rupture direction azimuth shown in the form of a rose diagram. Black colored diamond indicates the updip direction obtained from the mean values of the focal mechanisms. (b) and (c): Relationships between the rupture direction azimuths and moment magnitude and centroid depth, respectively, colored according to the rupture azimuth scale in (d). Diamonds and vertical lines indicate the mean values and the 90 % confidential intervals based on bootstrap re-sampling, respectively, in each bin with the same number of events. (d): Map view showing the rupture direction azimuths. Blue contours show slip areas of large earthquakes from Nagai et al. (2001), Yamanaka and Kikuchi (2004), Iinuma et al. (2012), and Kubo and Nishikawa (2020). The dashed curve indicates

the northeastern limit of the Philippine Sea Plate (Uchida et al., 2009). The gray curve denotes the depth limit of interplate earthquakes on the Pacific plate (Igarashi et al., 2001; Uchida et al., 2009; Kita et al., 2010). (e)-(i): Frequency distributions of the rupture direction azimuths in the five latitude ranges as shown in (d).

The predominance of updip rupture was most comprehensible in the Iwate-Oki and Miyagi-Oki regions (Figs. 5f and g). The same tendency was also observed in the Fukushima and Ibaraki-Oki regions (Fig. 6h), which are located to the north of the northeastern limit of the Philippine Sea plate. In the northernmost region and the southernmost region (south of the northeastern limit of the Philippine Sea plate), the dominant rupture directions are SSE (Figs. 5e and i). Although this SSE direction is roughly consistent with the predominance of updip rupture, the fault-strike component is large.

4. Discussion

The results indicate that ruptures of most of the analyzed earthquakes primarily propagated in the updip direction. This tendency was noticed along the Japan trench at depths of 35–60 km. This systematic tendency suggests that rupture propagation is not governed by a random process or by the rupture history but instead it is due to permanent structures present in the system. This systematic tendency is difficult to explain using small-scale heterogeneities in stress, friction, material properties, and fault geometry. Large-scale properties (much larger than the fault size of an individual earthquake) are required to explain this widespread tendency. The effect of a bimaterial fault interface affects the earthquake rupture directions, where two blocks with different elastic properties are located across a fault (Weertman, 1980; Shi and Ben-Zion, 2006).

This model predicts that Mode-II subshear rupture tends to propagate in the direction of motion of the compliant side of the fault, which is supported by observations on the San Andreas Fault (Lengliné and Got, 2011) and laboratory experiments (Anooshehpoor and Brune, 1999). This study used interplate earthquakes that were mostly deeper than 30 km. In this depth range, the footwall material (oceanic crust) is more compliant than the hanging wall material, because the hanging wall is the mantle in this depth range (Ito et al., 2004). Therefore, the bimaterial effect predicts that earthquake ruptures will tend to propagate westward, which is the opposite of what we observed here. That is, the bimaterial effect alone cannot explain the results of this study.

Determining the cause of the rupture direction is difficult, but the depth dependencies of stress, friction, and pore pressure probably play essential roles in rupture dynamics in the Japan trench. A similar prevalence for updip rupture propagation has been reported for large interplate earthquakes in subduction zones (Kato and Seno, 2003; Chounet et al., 2018) and intraplate earthquakes near the base of the seismogenic zone (Sibson, 1982). One possible cause for the prevalence of updip rupture is a steady creep that occurs along the deeper portion of the plate boundary. The earthquakes analyzed in this study were mainly located near the lower limit of the seismogenic zone (gray curve in Fig. 5), beneath which the plate boundary dislocates aseismically. The contrast in slip velocity between the creeping region and the locked seismogenic patches increases the shear stress along the deeper edge of the locked patches. This facilitates rupture initiation near the deeper edge and propagation in the updip direction, given that the nucleation size is sufficiently smaller than the final rupture area (Kato and Seno, 2003). Numerical modeling of earthquake cycles has shown that some small earthquakes can nucleate near the rheological transition boundary and propagate in a non-preferred direction predicted by the bimaterial effect (Erickson and Day, 2016). Upward fluid flow along the plate boundary may play a similar role.

Submitted on Feb. 11, 2021

Fluids dehydrated from the subducting slab are suggested to migrate upward along the plate boundary because of the permeability anisotropy (Kawano et al., 2013; Sano et al., 2014). Higher pore pressures result in a higher reduction of fault strength along the deeper portion of the plate boundary. This may contribute to rupture initiation near the deeper edge of the locked patch and propagation in the updip direction. The updip ruptures may open up ways for fluids to migrate further upward along the plate interface.

The seismic patches of large earthquakes (M>7) are located in the updip region of the small earthquakes analyzed in this study (Fig. 5d). The updip ruptures of small earthquakes may redistribute the shear stress accumulated near the base of the seismogenic zone to the shallow seismic patches of large interplate earthquakes, thereby facilitating the occurrence of large earthquakes. Some of these small earthquakes may represent partial ruptures of the seismic patches of large earthquakes.

The dominant rupture direction has a significant fault-strike component in the northernmost (Fig. 5e) and the southernmost (Fig. 5i) regions. Since the trench axis bends near the northernmost region, the bending-related stress and structure may affect the rupture directions of earthquakes in this region. For the southernmost region, the Philippine Sea Plate subducts from the south, making the situation there different from the other areas. The seismic coupling substantially changes across the northern limit of the Philippines Sea plate (Uchida et al., 2009). The difference in material properties and the state of plate coupling may affect the rupture directivity in this region.

The predominance of updip rupture obtained in this study appears to be the opposite of the downdip ruptures reported for some large earthquakes (M >7) that occurred near the earthquakes analyzed in this study. Fig. 1(b) shows the hypocenters of the M ~7 interplate earthquakes near the earthquakes analyzed in this study. In the 2011 (M 7.4) Iwate-Oki and 2011 (M 7.6) Ibaraki-Oki earthquakes, the ruptures propagated in the updip direction (Kubo et al., 2013; Kubo and Nishikawa, 2020) were similar to the results presented herein. However, in the 1978 (M 7.4) and 2005 (M 7.2) Miyagi-Oki, and the 2008 (M 7.0) Ibaraki-Oki earthquakes, the ruptures were estimated to have propagated in the downdip direction (Wu et al., 2008; Takiguchi et al., 2011). The bimaterial effect, which facilitates downdip rupture along the deeper portion of the seismogenic zone, may be more dominant for larger earthquakes because the dynamic changes in normal stress increase with propagation distance (Shi and Ben-Zion, 2006). The competition between the bimaterial effect and other effects may cause diversity in the rupture directions of large earthquakes. The values of η estimated in this study ranged from 0.1 to 0.6, which are significantly smaller than the typical range of $V_\mathrm{r}/V_\mathrm{S}$ (0.6–0.9) (Geller, 1976). η corresponds to the actual value of $V_\mathrm{r}/V_\mathrm{S}$ only when the rupture is completely unilateral; otherwise, η should be smaller than the actual $V_\mathrm{r}/V_\mathrm{S}$ (Abercrombie et al., 2017). This is because the fit of the simple unilateral model cannot distinguish between slow and bilateral ruptures. The low values of η obtained in this study suggests that the earthquake ruptures along the Japan trench were directional, but not completely unilateral. η was variable, but appeared to decrease slightly with earthquake size from M_w 3.5 to 5 (Fig. 4b), which may reflect an enhanced bimaterial effect with magnitude that acts against the effect of deeper creep.

Alternatively, the apparent partial discrepancy in some large earthquake rupture directions may be due to temporal changes in the preferable rupture direction. Such a temporal change was reported after the 2004 Parkfield earthquake (Kane et al., 2003). Along the Tohoku-Oki plate boundary, the stress and frictional state were significantly perturbed by the 2011 (M 9) Tohoku-Oki earthquake. The results obtained in this study are for the period after the 2011 (M 9) Tohoku-Oki earthquake, while the three earthquakes with downdip ruptures (1978 and 2005 Miyagi-Oki and 2008 Ibaraki-Oki earthquakes) occurred before the 2011 Tohoku-Oki earthquake. In the Miyagi-Oki region, interplate earthquakes occurred in many offshore areas before the Tohoku-Oki earthquake, after which the offshore area was quiet and interplate earthquakes only occurred near the downdip limit of interplate earthquakes. This was probably due to the stress release and locking in the offshore region (e.g., Asano et al. 2011, Uchida and Matsuzawa, 2013). The 2011 Tohoku-Oki earthquake may have affected the preferential rupture direction of subsequent earthquakes, although it is not clear whether the effect of the Tohoku-Oki earthquake can explain the prevalence of updip rupture throughout the region. Unfortunately, the temporal changes in rupture directivity cannot be examined before and after the 2011 Tohoku-Oki earthquake using S-net data, as S-net was installed after the 2011 Tohoku-Oki earthquake. Fig. 3(c) shows the difficulty of estimating the rupture propagation direction using solely onland stations. However, the earthquake rupture directivities may be constrained solely by onland stations for few ideal cases (Figs. 2 and S1). To some extent, it may be possible to constrain the rupture directivities of small earthquakes along the Japan trench using only onland stations exclusively and assess the above hypothesis for future research.

The results presented herein indicate that the ruptures of most deep interplate earthquakes along the Japan trench had significant directivities. The prevalence of asymmetrical rupture has also been obtained for inland intraplate earthquakes in Japan (Yoshida, 2019). McGuire (2002) conducted global surveys of large earthquakes and concluded that unilateral rupture was predominant. Most studies of small to moderate-sized earthquakes along the Japan trench have been conducted mainly by assuming a non-directional model, including estimates of the earthquake stress drop (e.g., Yamada et al., 2021). However, the results of this study suggest that this assumption may be inappropriate for many interplate earthquakes. This issue may be reduced by incorporating the earthquake rupture directivity in the estimation method (Yoshida, 2019; Yoshida et al., 2019). The prevalence of asymmetrical rupture may enable the acquisition of detailed earthquake information that cannot be obtained if the directivity effects are ignored (e.g., fault orientation).

5. Conclusions

Prevalence of updip ruptures in small earthquakes was observed near the base of the seismogenic zone along the Japan trench. This updip rupture propagation tendency cannot be explained by the effect of a bimaterial interface; instead, the results suggest that deep, steady creep largely affects earthquake ruptures in subduction zones, although upward fluid flow along the plate boundary may also contribute to the ruptures. The updip ruptures redistribute the shear stress accumulated near the base of the seismogenic zone to shallow large seismic patches. Also, the updip ruptures may open up ways for fluids to migrate further upward along the plate interface. They may facilitate the occurrence of shallow megathrust earthquakes. A similar updip rupture propagation tendency was reported for large intraplate earthquakes near the base of the seismogenic zone. However, this study unambiguously demonstrates a similar trend in many small to moderate-sized interplate earthquakes obtained from both land-based and offshore seismic networks.

The present study could scarcely examine shallow interplate earthquakes ($z < 30$ km) that occurred far from the land, due to the difficulty in finding appropriate EGF events for the earthquakes. The stress release by the Tohoku-Oki earthquake reduces seismicity there. Studies in the future may be able to examine the rupture characteristics of shallow interplate earthquakes by detecting more offshore earthquakes and improving the location accuracy based on the seafloor observation data.

Acknowledgments

This study used hypocenters and S-wave arrival time data reported in the JMA unified catalog. The seismograms were collected and stored by JMA, national universities, and NIED (http://www.hinet.bosai.go.jp/?LANG=en). The figures were created using GMT (Wessel and Smith, 1998). KY thanks Toru Matsuzawa and Kazuya Tateiwa for discussions about the velocity contrast across the Tohoku-Oki plate boundary. This research was supported by JSPS KAKENHI (Grant Numbers JP 17KK0081 and 20K14569).

References

Abercrombie, R.E., 2015. Investigating uncertainties in empirical Green's function analysis of earthquake source parameters. J. Geophys. Res. Solid Earth 120, 1–15. https://doi.org/10.1002/2015JB011984.Received

Abercrombie, R.E., Poli, P., Bannister, S., 2017. Earthquake Directivity, orientation and stress drop within the subducting plate at the Hikurangi margin, New Zealand. J. Geophys. Res. Solid Earth. https://doi.org/10.1002/2017JB014935

Akaike, H., 1974. A New Look at the Statistical Model Identification. IEEE Trans. Automat. Contr. 19, 716–723. https://doi.org/10.1109/TAC.1974.1100705

Aki, K., 1967. Scaling law of seismic spectrum. J. Geophys. Res. 72, 1217–1231. https://doi.org/10.1029/JZ072i004p01217

Andrews, D.J., 1976. RUPTURE VELOCITY OF PLANE STRAIN SHEAR CRACKS. J Geophys Res 81, 5679–5687. https://doi.org/10.1029/JB081i032p05679

Andrews, D.J., 2013. Objective Determination of Source Parameters and Similarity of Earthquakes of Different Size. pp. 259–267. https://doi.org/10.1029/gm037p0259

Anooshehpoor, A., Brune, J.N., 1999. Wrinkle-like Weertman pulse at the interface between two blocks of foam rubber with different velocities. Geophys. Res. Lett. 26, 2025–2028. https://doi.org/10.1029/1999GL900397

Aoi, S., Asano, Y., Kunugi, T., Kimura, T., Uehira, K., Takahashi, N., Ueda, H., Shiomi, K., Matsumoto, T., Fujiwara, H., 2020. MOWLAS: NIED observation network for earthquake, tsunami and volcano. Earth, Planets Sp. 72. https://doi.org/10.1186/s40623-020-01250-x

Asano, Y., Saito, T., Ito, Y., Shiomi, K., Hirose, H., 2011. Spatial distribution and focal mechanisms of aftershocks of the 2011 off the Pacific coast of Tohoku Earthquake. Earth, Planets Sp. 63, 669–673. https://doi.org/10.5047/eps.2011.06.016

Chounet, A., Vallée, M., Causse, M., Courboulex, F., 2018. Global catalog of earthquake rupture velocities shows anticorrelation between stress drop and rupture velocity. Tectonophysics

733, 148–158. https://doi.org/10.1016/j.tecto.2017.11.005

Erickson, B.A., Day, S.M., 2016. Bimaterial effects in an earthquake cycle model using rate-and-state friction. J. Geophys. Res. Solid Earth 121, 2480–2506. https://doi.org/10.1002/2015JB012470

Geller, R.J., 1976. Scaling relations for earthquake source parameters and magnitudes. Bull. Seismol. Soc. Am. 66, 1501–1523.

Harris, R.A., Day, S.M., 2005. Material contrast does not predict earthquake rupture propagation direction. Geophys. Res. Lett. 32, 1–4. https://doi.org/10.1029/2005GL023941

Hasegawa, A., Yoshida, K., Asano, Y., Okada, T., Iinuma, T., Ito, Y., 2012. Change in stress field after the 2011 great Tohoku-Oki earthquake. Earth Planet. Sci. Lett. 355–356, 231–243. https://doi.org/10.1016/j.epsl.2012.08.042

Haskell, N.A., 1964. Total energy and energy spectral density of elastic wave radiation from propagating faults. Bull. Seismol. Soc. Am. 54, 1811–1841.

Igarashi, T., Matsuzawa, T., Umino, N., Hasegawa, A., 2001. Spatial distribution of focal mechanisms for interplate and intraplate earthquakes associated with the subducting Pacific plate beneath the northeastern Japan arc: A triple-planed deep seismic zone. J. Geophys. Res. Solid Earth 106, 2177–2191. https://doi.org/10.1029/2000jb900386

Iinuma, T., Hino, R., Kido, M., Inazu, D., Osada, Y., Ito, Y., Ohzono, M., Tsushima, H., Suzuki, S., Fujimoto, H., Miura, S., 2012. Coseismic slip distribution of the 2011 off the Pacific Coast of Tohoku Earthquake (M9.0) refined by means of seafloor geodetic data. J. Geophys. Res. Solid Earth 117. https://doi.org/10.1029/2012JB009186

Ito, A., Fujie, G., Tsuru, T., Kodaira, S., Nakanishi, A., Kaneda, Y., 2004. Fault plane geometry in the source region of the 1994 Sanriku-oki earthquake. Earth Planet. Sci. Lett. 223, 163–175. https://doi.org/10.1016/j.epsl.2004.04.007

Kagan, Y.Y., 1991. 3-D rotation of double-couple earthquake sources. Geophys. J. Int. 106, 709–716. https://doi.org/10.1111/j.1365-246X.1991.tb06343.x

Kanamori, H., Anderson, D., 1975. Theoretical basis of some empirical relations in seismology. Bull. Seismol. Soc. Am. 65, 1073–1095.

Kane, D.L., Shearer, P.M., Goertz-Allmann, B.P., Vernon, F.L., 2013. Rupture directivity of small earthquakes at Parkfield. J. Geophys. Res. Solid Earth 118, 212–221. https://doi.org/10.1029/2012JB009675

Kato, N., Seno, T., 2003. Hypocenter depths of large interplate earthquakes and their relation to seismic coupling. Earth Planet. Sci. Lett. 210, 53–63. https://doi.org/10.1016/S0012-821X(03)00141-9

Kawano, S., Katayama, I., Okazaki, K., 2011. Permeability anisotropy of serpentinite and fluid pathways in a subduction zone. Geology 39, 939–942. https://doi.org/10.1130/G32173.1

Kita, S., Okada, T., Hasegawa, A., Nakajima, J., Matsuzawa, T., 2010. Anomalous deepening of a seismic belt in the upper-plane of the double seismic zone in the Pacific slab beneath the Hokkaido corner: Possible evidence for thermal shielding caused by subducted forearc crust materials. Earth Planet. Sci. Lett. 290, 415–426. https://doi.org/10.1016/j.epsl.2009.12.038

Kubo, H., Asano, K., Iwata, T., 2013. Source-rupture process of the 2011 Ibaraki-oki, Japan, earthquake (M w 7.9) estimated from the joint inversion of strong-motion and GPS Data: Relationship with seamount and Philippine Sea Plate. Geophys. Res. Lett. 40, 3003–3007. https://doi.org/10.1002/grl.50558

Kubo, H., Nishikawa, T., 2020. Relationship of preseismic, coseismic, and postseismic fault ruptures of two large interplate aftershocks of the 2011 Tohoku earthquake with slow-earthquake activity. Sci. Rep. 10. https://doi.org/10.1038/s41598-020-68692-x

Lengliné, O., Got, J.L., 2011. Rupture directivity of microearthquake sequences near Parkfield, California. Geophys. Res. Lett. 38. https://doi.org/10.1029/2011GL047303

Ligorría, J.P., Ammon, C.J., 1999. Iterative deconvolution and receiver-function estimation. Bull. Seismol. Soc. Am. 89, 1395–1400.

McGuire, J.J., Zhao, L., Jordan, T.H., 2002. Predominance of unilateral rupture for a global catalog of large earthquake. Bull. Seismol. Soc. Am. 92, 3309–3317. https://doi.org/10.1785/0120010293

Nagai, R., Kikuchi, M., Yamanaka, Y., 2001. Comparative Study on the Source Processes of Recurrent Large Earthquakes in Sanriku-oki Region: the 1968 Tokachi-oki Earthquake and the 1994 Sanriku-oki Earthquake. Zisin (Journal Seismol. Soc. Japan. 2nd ser.) 54, 267–280. https://doi.org/10.4294/zisin1948.54.2_267

Nakajima, J., Hirose, F., Hasegawa, A., 2009. Seismotectonics beneath the Tokyo metropolitan area, Japan: Effect of slab-slab contact and overlap on seismicity. J. Geophys. Res. Solid Earth 114, B08309. https://doi.org/10.1029/2008JB006101

National Research Institute for Earth Science and Disaster Resilience (2019a). NIED Hi-net. Natl. Res. Inst. Earth Sci. Disaster Resil.,doi:10.17598/NIED.0003

National Research Institute for Earth Science and Disaster Resilience (2019c). NIED F-net. Natl. Res. Inst. Earth Sci. Disaster Resil.,doi:10.17598/NIED.0005

National Research Institute for Earth Science and Disaster Resilience (2019d). NIED V-net. Natl. Res. Inst. Earth Sci. Disaster Resil., doi:10.17598/NIED.0006

National Research Institute for Earth Science and Disaster Resilience (2019d). NIED S-net. Natl. Res. Inst. Earth Sci. Disaster Resil., doi:10.17598/NIED.0007

Sano, Y., Hara, T., Takahata, N., Kawagucci, S., Honda, M., Nishio, Y., Tanikawa, W., Hasegawa, A., Hattori, K., 2014. Helium anomalies suggest a fluid pathway from mantle to trench during the 2011 Tohoku-Oki earthquake. Nat. Commun. 5. https://doi.org/10.1038/ncomms4084

Sato, T., Hirasawa, T., 1973. Body wave spectra from propagating shear cracks. J. Phys. Earth. https://doi.org/10.4294/jpe1952.21.415

Shi, Z., Ben-Zion, Y., 2006. Dynamic rupture on a bimaterial interface governed by slip-weakening friction. Geophys. J. Int. 165, 469–484. https://doi.org/10.1111/j.1365-246X.2006.02853.x

Sibson, R.H., 1983. Continental fault structure and the shallow earthquake source. J. Geol. Soc.

London. 140, 741–767. https://doi.org/10.1144/gsjgs.140.5.0741

Takagi, R., Uchida, N., Nakayama, T., Azuma, R., Ishigami, A., Okada, T., Nakamura, T., Shiomi, K., 2019. Estimation of the Orientations of the S-net Cabled Ocean-Bottom Sensors. Seismol. Res. Lett. 90, 2175–2187. https://doi.org/10.1785/0220190093

Takiguchi, M., Asano, K., Iwata, T., 2011. The Comparison of Source Models of Repeating Subduction-zone Earthquakes Estimated Using Broadband Strong Motion Records-1982 and 2008 Ibaraki-ken-oki M7 Earthquakes-. Zisin (Journal Seismol. Soc. Japan. 2nd ser.). https://doi.org/10.4294/zisin.63.223

Uchida, N., Nakajima, J., Hasegawa, A., Matsuzawa, T., 2009. What controls interplate coupling?: Evidence for abrupt change in coupling across a border between two overlying plates in the NE Japan subduction zone. Earth Planet. Sci. Lett. 283, 111–121. https://doi.org/10.1016/j.epsl.2009.04.003

Uchida, N., Matsuzawa, T., 2013. Pre- and postseismic slow slip surrounding the 2011 Tohoku-oki earthquake rupture. Earth Planet. Sci. Lett. 374, 81–91. https://doi.org/10.1016/j.epsl.2013.05.021

Weertman, J., 1980. Unstable slippage across a fault that separates elastic media of different elastic constants. J. Geophys. Res. 85, 1455. https://doi.org/10.1029/JB085iB03p01455

Wu, C., Koketsu, K., Miyake, H., 2008. Source processes of the 1978 and 2005 Miyagi-oki, Japan earthquakes: Repeated rupture of asperities over successive large earthquakes. J. Geophys. Res. Solid Earth 113. https://doi.org/10.1029/2007JB005189

Yamada, T., Duan, M., Kawahara, J., 2021. Spatio-temporal characteristics of frictional properties on the subducting Pacific Plate off the east of Tohoku district, Japan estimated from stress drops of small earthquakes. Earth, Planets Sp. 73. https://doi.org/10.1186/s40623-020-01326-8

Yamanaka, Y., Kikuchi, M., 2004. Asperity map along the subduction zone in northeastern Japan inferred from regional seismic data. J. Geophys. Res. Solid Earth 109.

https://doi.org/10.1029/2003JB002683

Ye, L., Lay, T., Kanamori, H., Rivera, L., 2016. Rupture characteristics of major and great (Mw ≥ 7.0) megathrust earthquakes from 1990 to 2015: 1. Source parameter scaling relationships. J. Geophys. Res. Solid Earth 121, 826–844. https://doi.org/10.1002/2015JB012426

Yoshida, K., 2019. Prevalence of asymmetrical rupture in small earthquakes and its effect on the estimation of stress drop: a systematic investigation in inland Japan. Geosci. Lett. 6. https://doi.org/10.1186/s40562-019-0145-z

Yoshida, K., Saito, T., Emoto, K., Urata, Y., Sato, D., 2019. Rupture directivity, stress drop, and hypocenter migration of small earthquakes in the Yamagata-Fukushima border swarm triggered by upward pore-pressure migration after the 2011 Tohoku-Oki earthquake. Tectonophysics 769. https://doi.org/10.1016/j.tecto.2019.228184